Progress In Electromagnetics Research C, Vol. 136, 123–135, 2023

Balanced-to-Unbalanced Bagley Power Divider with Input-Reflectionless Filtering Characteristics

Qi Chen, Zhongbao Wang*, Shipeng Zhao, Hongmei Liu, and Shaojun Fang

Abstract—A novel balanced-to-unbalanced (BTU) Bagley power divider (BPD) with input-reflectionless filtering characteristics is proposed. It features a balanced input port and three single-ended output ports, which is difficult to achieve by means of conventional BTU power dividers. The filtering characteristics are achieved by parallel coupled lines. To further improve the differential-mode filtering selectivity, stepped impedance resonators are applied to introduce two transmission zeros near the passband. The input-reflectionless characteristic in the bandstop region is achieved by loading absorptive branches. For verifying the proposed power divider topology, a prototype of microstrip BTU Bagley power divider operating at 1.0 GHz is designed and fabricated with 3-dB filtering bandwidth of 72%. Furthermore, 10-dB input-reflectionless bandwidth covers the full measurement frequency from 0 to 2.5 GHz. Good agreement between the simulation and measurement validated the proposed method.

1. INTRODUCTION

Power dividers (PDs) are very important basic microwave components in various wireless communication systems [1]. Bagley power divider (BPD) is one of the planar microwave dividers that have attracted much attention recently. The BPD has several advantages over the other types of power dividers. Specifically, BPDs do not use lumped elements and can be easily extended to any number of output ports [2]. The development of BPDs [3–6] has advanced significantly in recent years. However, all these developments are based on single-ended types of PDs. Due to their benefits of differential-mode (DM) signal transmission, excellent common-mode (CM) suppression, high immunity to environmental noise, and ease of connecting with other balanced circuits [7], balanced power dividers have been utilized extensively in systems [8–10]. Subsequently, with the rapid development of miniaturization and integration of high-speed electronic systems, different kinds of balanced-to-balanced (BTB) filtering power dividers (FPDs) have been extensively studied [11–13].

Compared to BTB PDs, balanced-to-unbalanced (BTU) PDs also have the capability to suppress the CM noise [14–20]. Furthermore, BTU PD has the advantage that it can be connected with single-ended and balanced circuits at the same time. In [14], a BTU Wilkinson power divider was proposed, which used short-terminated four-wire coupled lines and a T-shaped cross section. But the 3-dB bandwidth is limited to only about 25%. In [15], by using three cascaded coupled lines and an isolation resistor, a compact wideband BTU out-of-phase PD was proposed. Subsequently, a BTU microstrip power divider based on coupled lines, which integrates a filtering function, was proposed [16]. Moreover, several BTU FPDs have also been studied [17–20]. A new BTU power divider was proposed to achieve a high level of CM rejection [17]. The filtering response is produced by loading shunt coupled-line stubs with numerous transmission zeros. In [18], a multifunctional broadband BTU FPD was reported, using a half-wavelength ring resonator and a coupled line section to achieve filtering performance. A high-selectivity BTU FPD using a dual-mode ring resonator was proposed [19]. The transmission zeros

Received 30 June 2023, Accepted 4 August 2023, Scheduled 15 August 2023
* Corresponding author: Zhongbao Wang (wangzb@dlmu.edu.cn).
The authors are with the School of Information Science and Technology, Dalian Maritime University, Dalian, Liaoning 116026, China.

near the passband can be easily changed by choosing different pairs of characteristic impedances of ring resonators, and additional transmission zeros can be introduced by the loaded stubs. In order to better meet the requirements of modern wireless communication systems for miniaturization of components, a miniaturized BTU FPD with a wide upper stopband was proposed [20].

However, all the aforementioned FPDs give rise to undesired RF power reflections in their stopbands that may deteriorate the active stages in the RF front ends. Instead of reflecting non-transmitted RF input signal energy back to the source, RF reflectionless or absorptive bandpass filters [21–23] absorb it in their stopbands. Therefore, reflectionless performance can be achieved by introducing the absorptive branch [24] and parallel LC resonators [25] at the input or output ports of the FPD. To the best of our knowledge, the BTU Bagley power divider with input-reflectionless filtering characteristics has not been reported before. Consequently, in order to solve the problems of differential input, filtering, and reflectionless of the above Bagley power divider, it is necessary to design a BTU BPD with input-reflectionless filtering characteristics.

In this paper, a BTU Bagley power divider with input-reflectionless filtering characteristics is proposed, which has the function of common-mode suppression (CMS) and more flexibility of connecting with single-ended or balanced circuits. The filtering characteristics are achieved by parallel coupled lines. To further improve the differential-mode filtering selectivity, stepped impedance resonators are applied to introduce two transmission zeros near the passband. The input-reflectionless characteristic in the bandstop region is achieved by loading absorptive branches. One microstrip prototype is fabricated and measured. The experimental results agree well with the theoretical and simulated ones.

2. THEORETICAL ANALYSIS AND DESIGN

The initial circuit of the proposed BTU Bagley power divider is shown in Fig. 1. The balanced input ports are defined by ports 1+ and 1−, and the unbalanced output ports are defined by port 2, port 3, and port 4 in Z_0. The mixed-mode scattering matrix ($\mathbf{S}_{\mathrm{mm}}$) can be extracted from the standard scattering matrix ($\mathbf{S}_{\mathrm{std}}$) using the matrix conversion, and the mixed-mode scattering matrix ($\mathbf{S}_{\mathrm{mm}}$) can

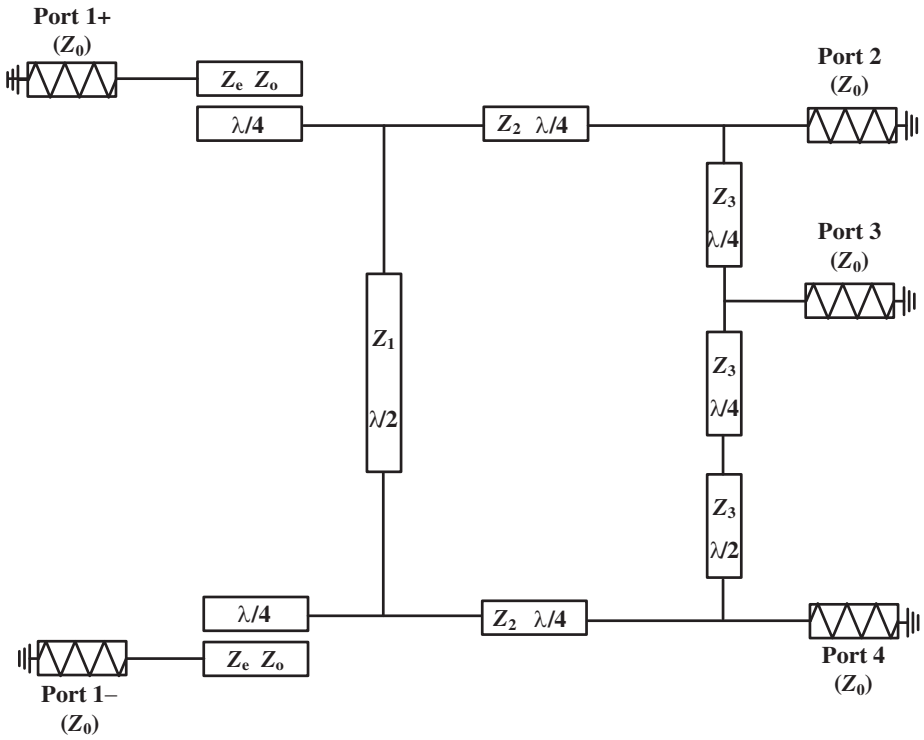

Figure 1. The initial circuit of the proposed BTU Bagley power divider.

be defined as [16]

$$\mathbf{S}_{\mathrm{mm}} = \begin{bmatrix} S_{\mathrm{dd11}} & S_{\mathrm{dc11}} & S_{\mathrm{ds12}} & S_{\mathrm{ds13}} & S_{\mathrm{ds14}} \\ S_{\mathrm{cd11}} & S_{\mathrm{cc11}} & S_{\mathrm{cs12}} & S_{\mathrm{cs13}} & S_{\mathrm{cs14}} \\ S_{\mathrm{sd21}} & S_{\mathrm{sc21}} & S_{\mathrm{ss22}} & S_{\mathrm{ss23}} & S_{\mathrm{ss24}} \\ S_{\mathrm{sd31}} & S_{\mathrm{sc31}} & S_{\mathrm{ss32}} & S_{\mathrm{ss33}} & S_{\mathrm{ss34}} \\ S_{\mathrm{sd41}} & S_{\mathrm{sc41}} & S_{\mathrm{ss42}} & S_{\mathrm{ss43}} & S_{\mathrm{ss44}} \end{bmatrix} \tag{1}$$

and

$$\begin{cases} S_{\mathrm{dd11}} = (S_{1+1+} - S_{1+1-} - S_{1-1+} + S_{1-1-})/2 \\ S_{\mathrm{cc11}} = (S_{1+1+} + S_{1+1-} + S_{1-1+} + S_{1-1-})/2 \\ S_{\mathrm{cd11}} = (S_{1+1+} - S_{1+1-} + S_{1-1+} + S_{1-1-})/2 \\ S_{\mathrm{dc11}} = (S_{1+1+} + S_{1+1-} - S_{1-1+} - S_{1-1-})/2 \end{cases} \tag{2a}$$

$$\begin{cases} S_{\mathrm{sd}n1} = (S_{n1+} - S_{n1-})/\sqrt{2} \\ S_{\mathrm{ds1}n} = (S_{1+n} - S_{1-n})/\sqrt{2} \\ S_{\mathrm{sc}n1} = (S_{n1+} + S_{n1-})/\sqrt{2} \\ S_{\mathrm{cs1}n} = (S_{1+n} + S_{1-n})/\sqrt{2} \end{cases} \tag{2b}$$

$$S_{\mathrm{ss}ij} = S_{ij} \tag{2c}$$

where the subscripts d, c, and s represent differential mode, common mode, and single-ended ports. In order to meet the requirements of ideal impedance matching, mode-conversion coefficient, and common-mode suppression, the following conditions (3) need to be realized.

$$S_{\mathrm{dd11}} = S_{\mathrm{dc11}} = S_{\mathrm{sc21}} = S_{\mathrm{sc31}} = S_{\mathrm{sc41}} = 0 \tag{3a}$$

$$S_{\mathrm{cc11}} = 1 \tag{3b}$$

2.1. Analysis of DM Impedance Matching

As shown in Fig. 1, the block diagram is composed of five transmission lines (Z_1, $\lambda/2$), (Z_2, $\lambda/4$) and (Z_3, $\lambda/4$), and two coupled lines with the even- and odd-mode characteristic impedances of Z_e and Z_o. To compensate the phase difference of the differential input, an additional $\lambda/2$ transmission line (Z_3) is added between ports 3 and 4.

Since the unbalanced port section is not a symmetric structure, the section before the unbalanced port is analyzed first, and this section is considered as a balanced-to-balanced filter, as shown in Fig. 2(a). When the odd-mode (i.e., differential-mode) signal is excited from ports 1+ and 1− in Fig. 2(a), the simplified odd-mode equivalent circuit is shown in Fig. 2(b). The A-matrix between ports 1+ and 2 of the odd-mode equivalent circuit can be calculated as

$$[A] = \begin{bmatrix} A_{11} & A_{12} \\ A_{21} & A_{22} \end{bmatrix} = [A]_{\mathrm{CL}} \times [A]_{\mathrm{TL1}} \times [A]_{\mathrm{TL2}} \tag{4}$$

where

$$[A]_{\mathrm{CL}} = \begin{bmatrix} \dfrac{c\cos\theta}{d} & \mathrm{j}\dfrac{d^2 - c^2\cos^2\theta}{2d\sin\theta} \\ \mathrm{j}\dfrac{2\sin\theta}{d} & \dfrac{c\cos\theta}{d} \end{bmatrix} \tag{5}$$

$$c = Z_{\mathrm{e}} + Z_{\mathrm{o}}, \quad d = Z_{\mathrm{e}} - Z_{\mathrm{o}}, \quad \theta = \frac{\pi f}{2f_0} \tag{6}$$

$$[A]_{\mathrm{TL1}} = \begin{bmatrix} 1 & 0 \\ \dfrac{1}{\mathrm{j}Z_1\tan\theta} & 1 \end{bmatrix} \tag{7}$$

$$[A]_{\mathrm{TL2}} = \begin{bmatrix} \cos\theta & \mathrm{j}Z_2\sin\theta \\ \dfrac{\mathrm{j}\sin\theta}{Z_2} & \cos\theta \end{bmatrix} \tag{8}$$

By applying Equations (5)–(8) into Equation (4), the final A-matrix of odd-mode equivalent circuit at the center frequency f_0 can be expressed as

$$[A] = \begin{bmatrix} A_{11} & A_{12} \\ A_{21} & A_{22} \end{bmatrix} = \begin{bmatrix} \dfrac{-d}{2Z_2} & \mathrm{j}\dfrac{Z_2 c}{d} \\ 0 & \dfrac{-2Z_2}{d} \end{bmatrix} \tag{9}$$

According to the transformation relationship between S-matrix and A-matrix, the S-parameter expressed in A-parameters is

$$S_{\mathrm{dd11}} = \frac{A_{11} + \dfrac{A_{12}}{Z_0} - A_{21}Z_0 - A_{22}}{A_{11} + \dfrac{A_{12}}{Z_0} + A_{21}Z_0 + A_{22}} \tag{10}$$

where Z_0 is the port impedance. Combining Equations (9) and (10), the final S_{dd11} of the whole circuit in Fig. 2(a) can be obtained as

$$S_{\mathrm{dd11}} = -\frac{4Z_0Z_2^2 - d^2Z_0 + cZ_2^2}{4Z_0Z_2^2 + d^2Z_0 - cZ_2^2} \tag{11}$$

In order to meet the requirement of input impedance matching (i.e., $S_{\mathrm{dd11}} = 0$), the following relationship can be obtained as

$$Z_2^2\left(4Z_0 + c\right) = d^2Z_0 \tag{12}$$

By applying Equations (6) into (12), we can get

$$Z_2^2\left(4Z_0 + Z_{\mathrm{e}} + Z_{\mathrm{o}}\right) = \left(Z_{\mathrm{e}} - Z_{\mathrm{o}}\right)^2 Z_0 \tag{13}$$

So the values of Z_{e}, Z_{o}, and Z_2 are selected appropriately to meet the input impedance matching of the differential mode signal.

When the even-mode (i.e., common-mode) signal is excited from ports 1+ and 1− in Fig. 2(a), the simplified even-mode equivalent circuit is shown in Fig. 2(c). The A-matrix between ports 1+ and 2 of the even-mode equivalent circuit can be calculated as

$$\begin{bmatrix} A & B \\ C & D \end{bmatrix} = \begin{bmatrix} \dfrac{c\cos\theta}{d} & \mathrm{j}\dfrac{d^2 - c^2\cos^2\theta}{2d\sin\theta} \\ \mathrm{j}\dfrac{2\sin\theta}{d} & \dfrac{c\cos\theta}{d} \end{bmatrix} \begin{bmatrix} 1 & 0 \\ \dfrac{1}{-\mathrm{j}Z_1\cot\theta} & 1 \end{bmatrix} \begin{bmatrix} \cos\theta & \mathrm{j}Z_2\sin\theta \\ \dfrac{\mathrm{j}\sin\theta}{Z_2} & \cos\theta \end{bmatrix} \tag{14}$$

According to the transformation relationship between S-matrix and A-matrix, we can get

$$S_{\mathrm{cc11}} = \frac{Z_0Z_1d^2 - 4Z_0Z_1Z_2^2 - 2Z_0Z_2^2c + Z_0Z_2d^2 + \mathrm{j}Z_2^2d^2\tan\theta}{Z_0Z_1d^2 + 4Z_0Z_1Z_2^2 + 2Z_0Z_2^2c + Z_0Z_2d^2 + \mathrm{j}Z_2^2d^2\tan\theta} \tag{15}$$

At the center frequency f_0, $\tan\theta = \infty$, then $S_{\mathrm{cc11}} = 1$, the common-mode signal is completely reflected.

2.2. Analysis of Power Dividing Ratio

To analyze the power dividing ratio, a simplified BTU BPD is shown in Fig. 3(a). When the balanced port 1 is excited by the differential-mode signals, they have the same amplitude and opposite phases. Moreover, it is assumed that all output ports have the same port impedance of Z_0, and the input impedance at port 1 is Z_{x}. When the signal passes through the $\lambda/2$ transmission line, the phase is inverted, and the impedance remains unchanged (i.e., $V_4 = -V_5$), so the schematic in Fig. 3(a) is simplified as shown in Fig. 3(b). It is assumed that the powers at port 2 and port 4 in Fig. 3(b) are always equal (i.e., $V_2 = V_4$), then this symmetry helps to draw the equivalent circuit as shown in

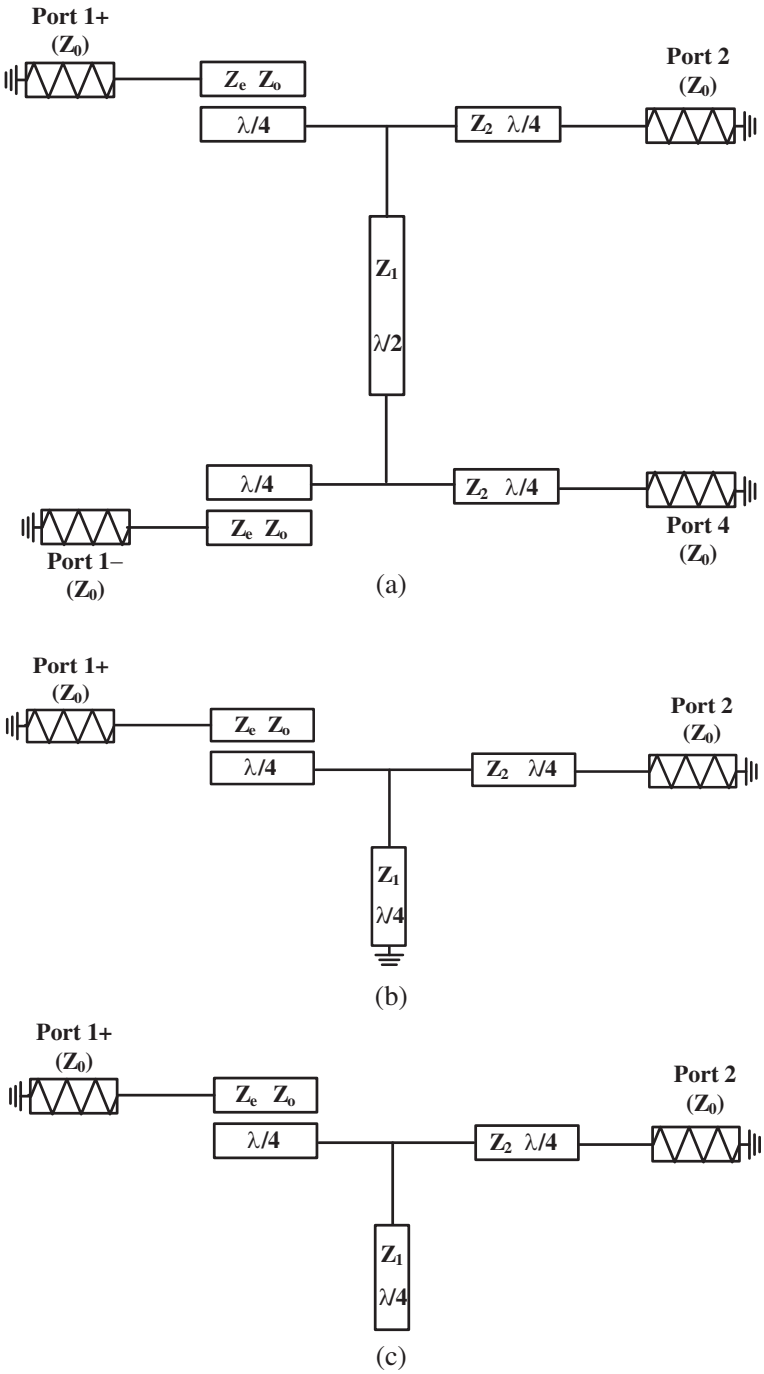

Figure 2. (a) Schematic of the equivalent balanced-to-balanced filter. (b) Odd-mode circuit. (c) Even-mode circuit.

Fig. 3(c). To analyze the equivalent BPD, Kirchhoff's current law (KCL) equation for each port (node) is first derived. Applying KCL at port 2,

$$I_2 = I_2' + I_2'' \tag{16}$$

Substitute the branch current equation into Equation (16) to obtain

$$\frac{V_1}{Z_{\mathrm{x}}} = \frac{\mathrm{j}V_3}{Z_3} + \frac{V_2}{Z_0} \tag{17}$$

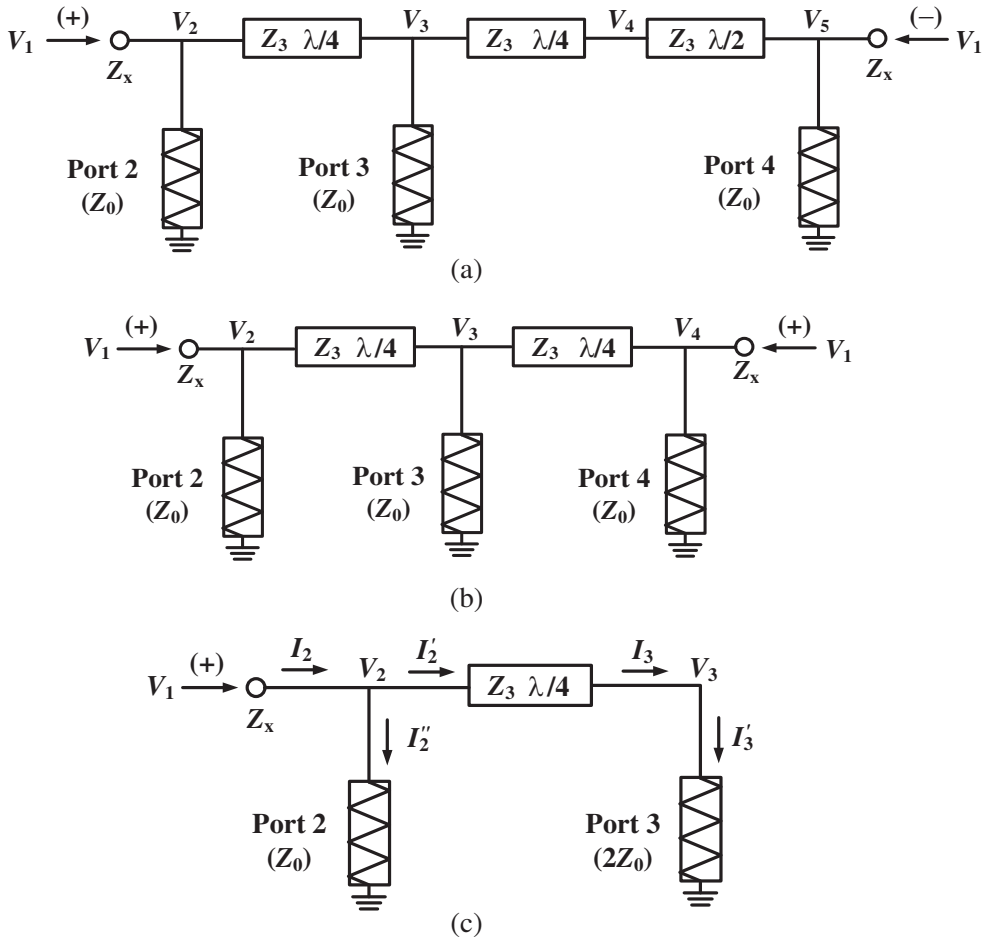

Figure 3. (a) BTU BPD. (b) Simplified circuit. (c) Equivalent circuit.

where

$$Z_{\mathrm{x}} = \frac{Z_0 Z_3^2}{2Z_0^2 + Z_3^2} \tag{18}$$

Likewise, using KCL at port 3,

$$I_3 = I_3' \tag{19}$$

The branch current equation can be substituted in Equation (19) to obtain Equation (20).

$$-\frac{\mathrm{j}V_2}{Z_3} = \frac{V_3}{2Z_0} \tag{20}$$

Equations (18) and (20) are used to derive the transmission coefficients of the BPD in question, from which the following equations are derived.

$$S_{21} = \frac{V_2}{V_1} = \frac{Z_0 Z_3^2}{Z_x\left(2Z_0^2 + Z_3^2\right)} \tag{21}$$

$$S_{31} = \frac{V_3}{V_1} = -\mathrm{j}\frac{2Z_0^2 Z_3}{Z_x\left(2Z_0^2 + Z_3^2\right)} \tag{22}$$

When port 1 inputs a unit power, the output powers are as follows,

$$P_2 = P_4 = |S_{21}|^2 = \frac{Z_0^2 Z_3^4}{Z_{\mathrm{x}}^2\left(2Z_0^2 + Z_3^2\right)^2} \tag{23}$$

$$P_3 = |S_{31}|^2 = \frac{4Z_0^4 Z_3^2}{Z_x^2 \left(2Z_0^2 + Z_3^2\right)^2} \tag{24}$$

At last, the power dividing ratio of BTU BPD is obtained as follows,

$$P_2 : P_3 : P_4 = 1 : 4\left(\frac{Z_0}{Z_3}\right)^2 : 1 \tag{25}$$

Note that the power dividing ratio controlled by the Z_3/Z_0 is only available near the center frequency, due to the properties of the $\lambda/4$ transmission line used in Fig. 3.

2.3. Enhancement of Filtering Characteristics

The schematic of the proposed BTU BPD with input-reflectionless filtering characteristics is depicted in Fig. 4. Compared with the BTU BPD shown in Fig. 1, it has two additional blocks. Fig. 5 depicts the simulated mixing S-parameters of the BTU BPD without blocks 1 and 2. When the center frequency $f_0 = 1\,\text{GHz}$ and the coupled lines have even- and odd-mode characteristic impedances of $Z_e = 140\,\Omega$ and $Z_o = 60\,\Omega$, S_{sd31} has two transmission zeros located at 0.49 and 1.51 GHz, respectively. This attributes to the signal interference of two upper and lower paths [26]. However, the filtering performances for S_{sd21} and S_{sd41} need to be further enhanced.

To improve the passband selectivity, transmission zeros are produced by two stepped-impedance resonators (SIRs) with characteristic impedance and length of (Z_4, $\lambda/4$) and (Z_5, $\lambda/4$) (i.e., Block 1 depicted by dash lines in Fig. 4), which are linked to the two unbalanced ports (i.e., ports 2 and 4). Fig. 6 shows the impacts of the proposed BTU BPD with and without stepped impedance resonators. It can be seen that SIR has only a slight effect on the in-band performance. By choosing the proper characteristic impedances Z_4 and Z_5, high selectivity and out-of-band rejection can be achieved. Furthermore,

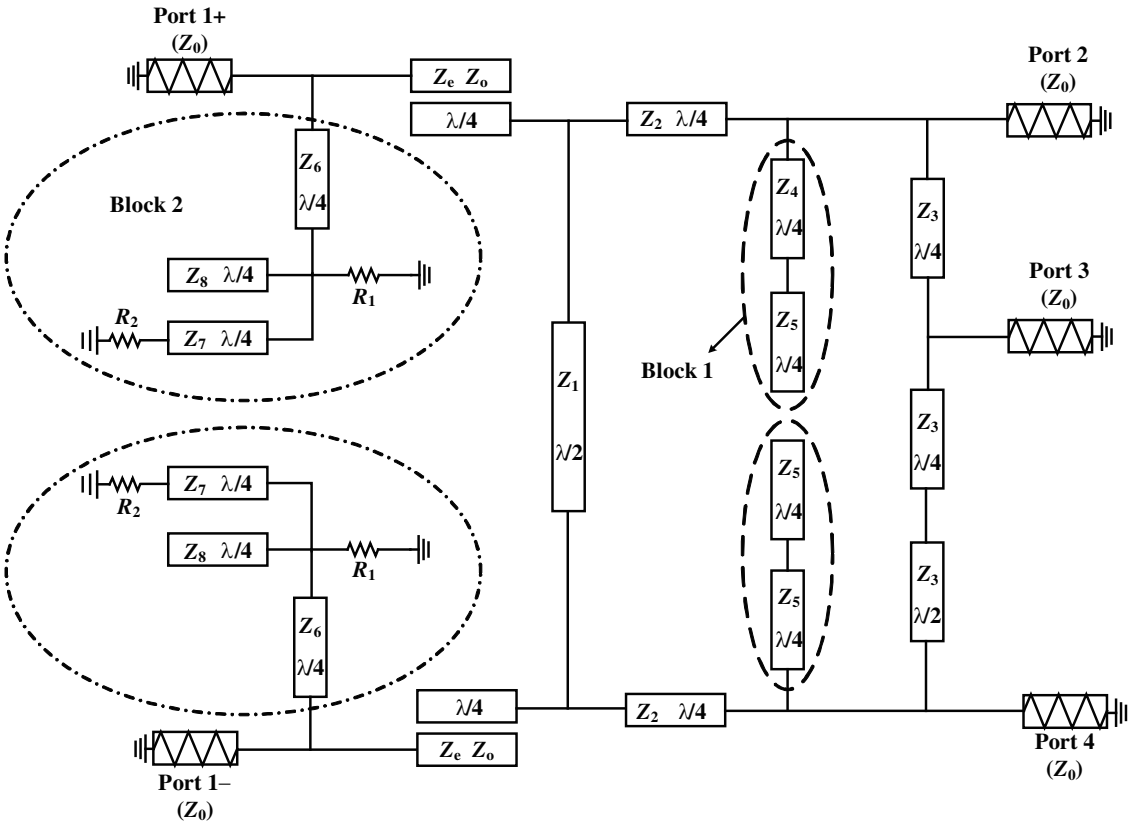

Figure 4. Schematic of the proposed BTU BPD with input-reflectionless filtering characteristics.

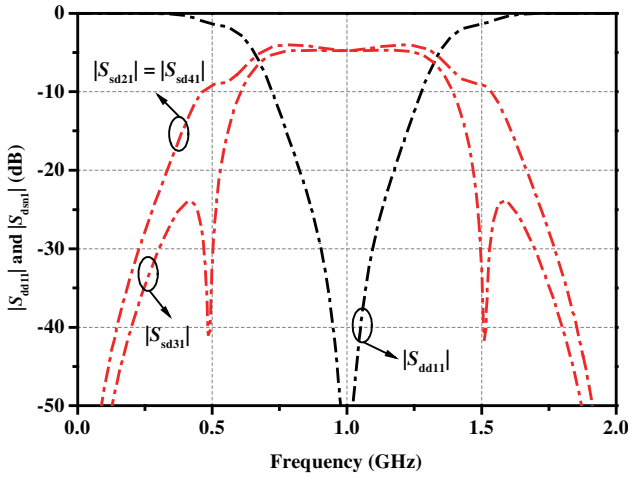

Figure 5. The simulated mixed S-parameters of the BTU BPD shown in Fig. 1.

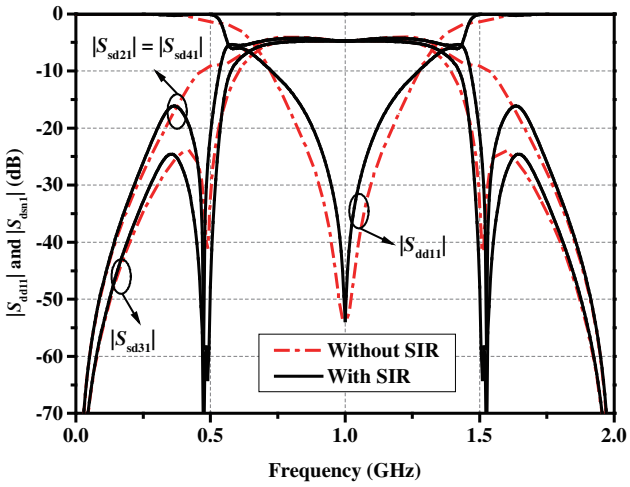

Figure 6. Simulated performances of the proposed BTU BPD with or without the SIR.

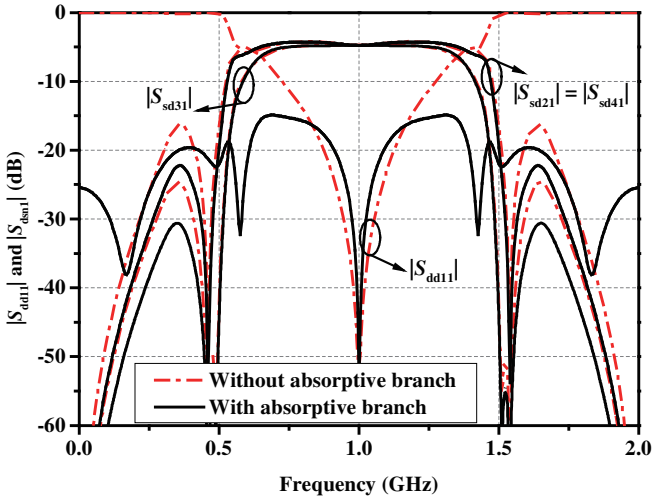

Figure 7. Simulated performances of the proposed BTU BPD with or without the absorptive branches.

considering the fabrication limitation of the width of the transmission lines, the transmission line impedance is within the range of $30 \sim 150\,\Omega$.

The effects of the proposed BTU BPD with and without absorptive branches are depicted in Fig. 7. To provide a reflectionless response at the input ports, two absorptive branches (i.e., Block 2 depicted by dash dot lines in Fig. 4) are linked to the balanced ports (i.e., ports 1+ and 1−). Each absorptive branch comprises two $\lambda/4$ transmission lines (Z_6 and Z_7), a $\lambda/4$ open stub (Z_8), and two absorbing resistors (R_1 and R_2). Because of the presence of the absorptive branches, some additional reflection zeros are created. It improves the matching bandwidth of $|S_{\mathrm{dd11}}|$, which is shown in Fig. 7. In addition, the added absorptive branch not only does not affect the location of the two transmission zeros, nor does it affect the in-band performance of the differential-mode transmission coefficient, but also increase the out-of-band rejection capability.

2.4. Design Procedure

Based on the above discussions and analysis, a simple design procedure of the proposed BTU BPD with input-reflectionless filtering characteristics can be summarized as follows.

1) Determine the power dividing ratio and port impedance, and calculate the value of Z_3 from Equation (25).

2) Calculate the value of Z_x from Equation (18), and subsequently select $Z_2 = Z_x$.

3) Calculate the values of Z_e and Z_o according to Equation (13) for obtaining ideal impedance matching characteristics at f_0.

4) Specify the filtering selectivity, and select the appropriate Z_4 and Z_5 for stepped impedance resonators.

5) Combining the input-reflectionless bandwidth, in-band return loss, and differential-mode out-of-band suppression, determine the absorptive branches.

3. IMPLEMENTATION AND PERFORMANCE

For verification, a microstrip BTU Bagley equal power divider with input-reflectionless filtering characteristics and the center frequency $f_0 = 1\,\text{GHz}$ is designed, fabricated, and measured. Based on the earlier analysis, the values of the electrical parameters obtained are shown in Table 1. The design is a planar structure, which can be fabricated using a simple single-layer printed circuit board, and its photograph is shown in Fig. 8. After optimization by Ansoft HFSS software, the final parameters are listed in Fig. 8(a). As depicted in Fig. 8(b), the prototype is realized with microstrip lines and fabricated on an F4B substrate with a thickness of 1.5 mm, dielectric constant of 2.65, and loss tangent of 0.003. The fabricated prototype is tested using an Agilent N5230A network analyzer.

Table 1. Electrical parameters of the proposed BTU BPD with input-reflectionless filtering characteristics.

Z_e (Ω)	Z_o (Ω)	Z_1 (Ω)	Z_2 (Ω)	Z_3 (Ω)	Z_4 (Ω)
140	60	36	33	100	115
Z_5 (Ω)	Z_6 (Ω)	Z_7 (Ω)	Z_8 (Ω)	R_1 (Ω)	R_2 (Ω)
70	82	145	45	76	110

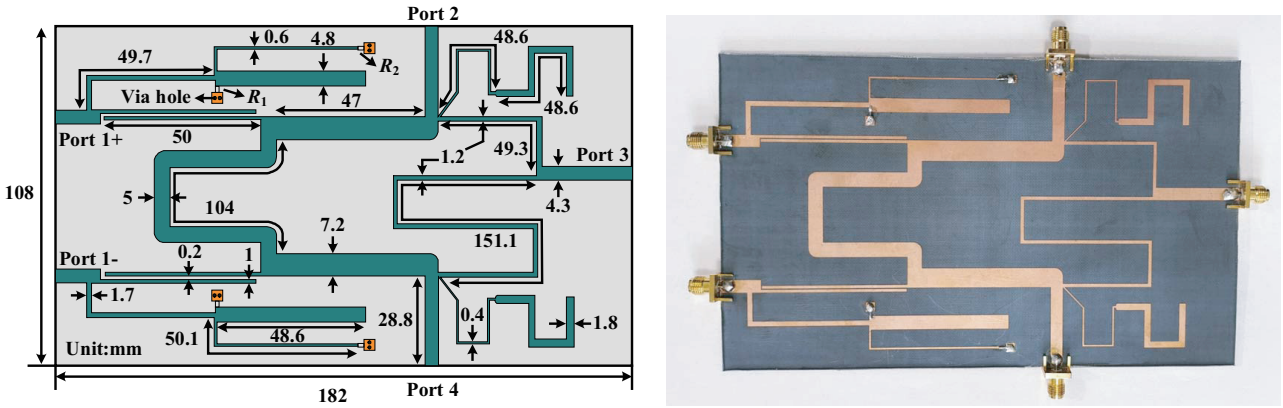

(a) (b)

Figure 8. (a) Layout and (b) photograph of the fabricated BTU BPD with input-reflectionless filtering characteristics.

Simulation and measurement curves of the proposed BTU BPD with input-reflectionless filtering characteristics in the $0 \sim 2.5\,\text{GHz}$ range are given in Fig. 9. For the balanced-port responses, the differential-mode return loss is greater than 10 dB (i.e., $|S_{dd11}| < -10\,\text{dB}$) at all frequencies, achieving wideband input-reflectionless characteristics in Fig. 9(a). In addition, the measured mode-conversion coefficient $|S_{dc11}|$ is less than $-20\,\text{dB}$. Fig. 9(b) is the measured and simulated results under DM signal

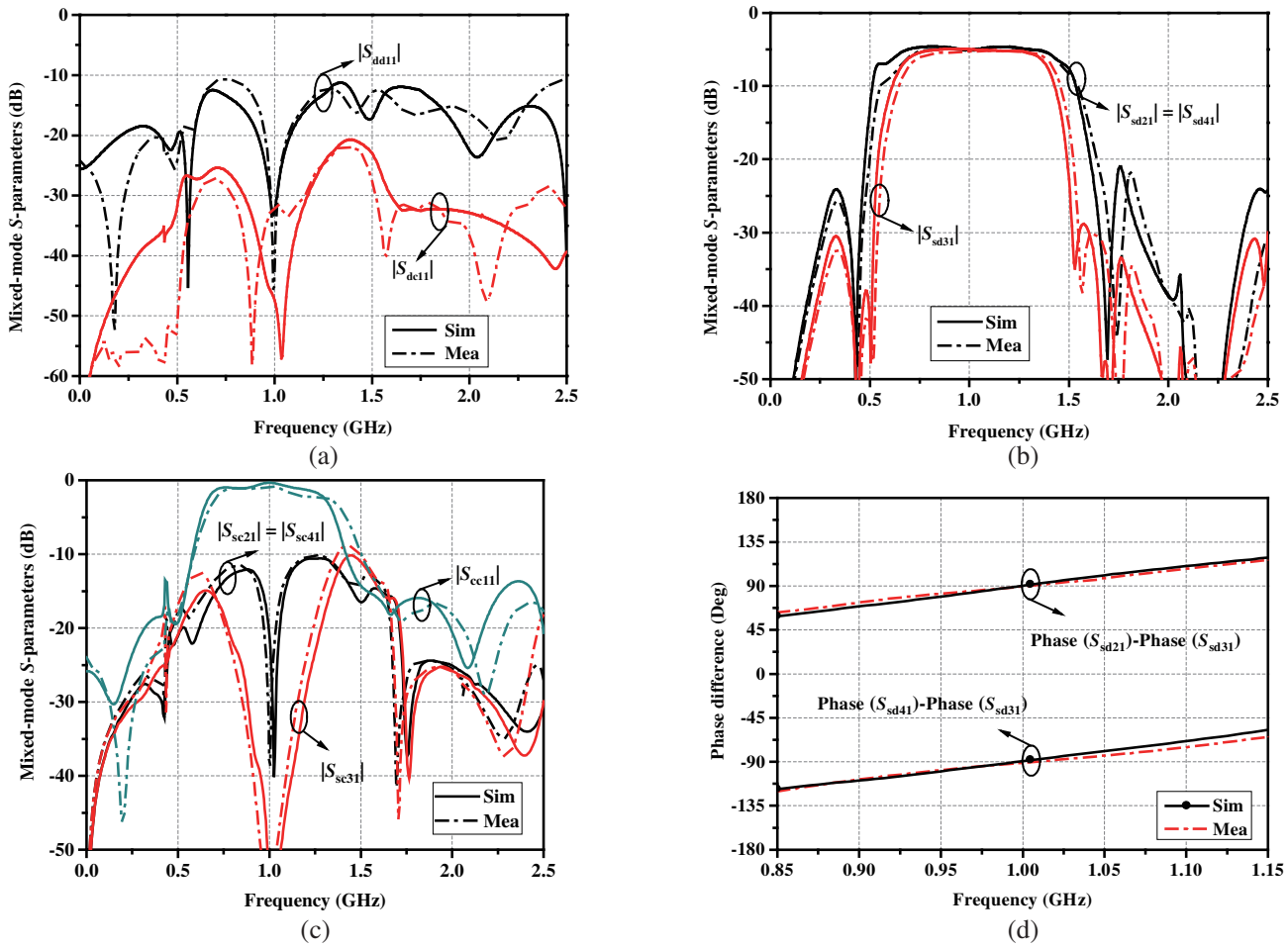

Figure 9. Simulated and measured results of the proposed BTU BPD with input-reflectionless filtering characteristics. (a) Balanced-port responses. (b) DM responses. (c) CM responses. (d) Phase difference.

excitation at the balanced port 1. The insertion loss including the power division loss for the three outputs is 5.2 ± 0.3 dB, and the measured 3-dB filtering bandwidth (FBW) is 72% (0.675 $\sim$ 1.435 GHz). DM to 3-port transmission coefficient $|S_{\mathrm{sd31}}|$ introduces four transmission zeros at 0.44, 0.51, 1.56, and 1.76 GHz, respectively, DM to 2-port (4-port) transmission coefficient $|S_{\mathrm{sd21}}|$ ($|S_{\mathrm{sd41}}|$) introduces two transmission zeros at 0.44 and 1.74 GHz, respectively, improving the filtering performance. Meanwhile, the DM out-of-band rejection is better than 20 dB. For the CM signal excitation in Fig. 9(c), the measured CM to 3-port transmission coefficient $|S_{\mathrm{sc31}}|$ is less than -8.9 dB with the greatest 60-dB CMS at the center frequency, and the measured CM to 2-port (4-port) transmission coefficient $|S_{\mathrm{sc21}}|$ ($|S_{\mathrm{sc41}}|$) is less than -10 dB with the greatest 47-dB CMS at the center of frequency. In the stopband, the measured CM reflection coefficient $|S_{\mathrm{cc11}}|$ is below -10 dB from 0 to 0.58 GHz and from 1.5 to 2.5 GHz. As shown in Fig. 9(d), the measured and simulated phase differences between the output ports 2 and 3 at f_0 are $90^\circ \pm 1^\circ$, and the phase differences between the output ports 3 and 4 are $-90^\circ \pm 1^\circ$.

The comparisons of the proposed BTU BPD with previous works are summarized in Table 2. This work is the first design of a BTU input-reflectionless filtering Bagley power divider. Compared with the reported power divider, the proposed BTU BPD has a wide filtering band and a good CM noise suppression level. Furthermore, input-reflectionless filtering characteristics have been integrated into the designed structure, which can protect the active stages in the RF front ends from undesired RF power reflection interference.

Table 2. Performance comparisons between the proposed BTU BPD and previous power divider.

Reference	f_0 (GHz)	Type	Number of output ports	FBW (%)	CMS (dB)	Input-reflectionless filtering
[4]	6.3	Single-ended Bagley	3	121.6	-	No
[9]	3.5	BTU DR	2	2.2	20	No
[14]	2.0	BTU Wilkinson	2	25	40	No
[15]	1.8	BTU Gysel	2	37.2	32	No
[16]	2.0	BTU Gysel	2	80	40	No
[17]	4.0	BTU Gysel	2	47.2	35	No
[24]	1.2	Single-ended Wilkinson	2	7.5	-	Yes
This work	1.0	BTU Bagley	3	72	47	Yes

DR: dielectric resonator.

4. CONCLUSIONS

In this paper, a novel BTU BPD with input-reflectionless filtering characteristics has been presented. The wideband input-reflectionless characteristics for the balanced port with DM excitation have been achieved by loading absorptive branches, where the differential-mode return loss is greater than 10 dB at all the measurement frequencies from 0 to 2.5 GHz. By using the stepped impedance resonator, two transmission zeros can be obtained near the passband to further enhance the filtering selectivity. Compared with the existing BPDs, the advantages of the proposed BTU BPD are DM signal transmission, good CMS, wideband input-reflectionless filtering, and the ability to connect to single-ended and balanced circuits. Furthermore, it can be applied in sequential three-feed circularly-polarized patch antenna [27] and three-way sequential power amplifier [28, 29] to add input-reflectionless filtering function and suppress the common-mode interference.

ACKNOWLEDGMENT

This work was supported by the National Natural Science Foundation of China (No. 61871417), the LiaoNing Revitalization Talents Program (No. XLYC2007024), and the Fundamental Research Funds for the Central Universities (No. 3132023243).

REFERENCES

1. Pozar, D. M., *Microwave Engineering*, 2nd Edition, Wiley, New York, NY, USA, 1998.
2. Shamaileh, K., A. Qaroot, and N. Dib, "Design of miniaturized 3-way Bagley polygon power divider using non-uniform transmission lines," *IEEE Int. Symp. Antenna & Prop.*, 29–32, Jul. 2011.
3. Saleh, S., W. Ismail, I. S. Z. Abidina, et al., "Compact UWB 1:2:1 unequal-split 3-way Bagley power divider using non-uniform transmission lines," *Journal of Electromagn. Waves and Appl.*, Vol. 35, No. 2, 262–276, Jan. 2021.
4. Dong, G. and X. Yang, "General design equations for arbitrary odd-way filtering Bagley polygon power divider with notch band," *Journal of Electromagn. Waves and Appl.*, Vol. 36, No. 3, 378–387, Aug. 2021.
5. Buesa-Zubiria, A. and J. Esteban, "Design of five-way Bagley polygon power dividers in rectangular waveguide," *IEEE Trans. Microwave Theory Tech.*, Vol. 66, No. 1, 116–127, Jan. 2018.

6. Jaradat, H., N. Dib, and K. Al Shamaileh, "Design of multi-band miniaturized Bagley power dividers based on non-uniform coplanar waveguide," *AEU — Int. J. Electron. Commun.*, Vol. 118, Art. No. 153137, May 2020.
7. Li, W. T., H. R. Zhang, X. J. Chai, et al.,, "Compact dual-band balanced-to-unbalanced filtering power divider design with extended common-mode suppression bandwidth," *IEEE Microwave Wireless Compon. Lett.*, Vol. 32, No. 6, 511–514, Jun. 2022.
8. Xia, B., L. S. Wu, and J. Mao, "A new balanced-to-balanced power divider/combiner," *IEEE Trans. Microwave Theory Tech.*, Vol. 60, No. 9, 2791–2798, Sep. 2012.
9. Li, H. Y., J. X. Xu, and X. Y. Zhang, "Miniaturized balanced filtering power dividers with arbitrary power division ratio using multimode dielectric resonator in single cavity," *IEEE Trans. Circuits Syst. II Exp. Briefs*, Vol. 69, No. 6, 2707–2711, Jun. 2022.
10. Xia, B., L. S. Wu, S. W. Ren, and J. F. Mao, "A balanced-to-balanced power divider with arbitrary power division," *IEEE Trans. Microwave Theory Tech.*, Vol. 61, No. 8, 2831–2841, Aug. 2013.
11. Zhang, G., Q. Zhang, Q. Liu, W. Tang, and J. Yang, "Design of a new dual-band balanced-to-balanced filtering power divider based on the circular microstrip patch resonator," *IEEE Trans. Circuits Syst. II Exp. Briefs*, Vol. 68, No. 12, 3542–3546, Dec. 2021.
12. Chen, S., W. C. Lee, and T. L. Wu, "Balanced-to-balanced and balanced-to-unbalanced power dividers with ultra-wideband common-mode rejection and absorption based on mode-conversion approach," *IEEE Trans. on Electromagn. Compat.*, Vol. 9, No. 2, 306–316, Feb. 2019.
13. Wei, F., Z. J. Yang, and P. Y. Qin, et al., "A balanced-to-balanced in-phase filtering power divider with high selectivity and isolation," *IEEE Trans. Microwave Theory Tech.*, Vol. 67, No. 2, 683–694, Feb. 2019.
14. Wu, L. S., Y. X. Guo, L. F. Qiu, and J. F. Mao, "A new balanced-to-single-ended (BTSE) power divider," *IEEE Int. Wireless Symp.*, 1–4, Mar. 2014.
15. Zhang, W., Y. Wu, Y. Liu, F. M. Ghannouchi, and A. Hasan, "A wideband balanced-to-unbalanced coupled-line power divider," *IEEE Microw. Wireless Compon. Lett.* Vol. 26, No. 6, 410–412, Jun. 2016.
16. Gao, X., W. Feng, W. Che, and Q. Xue, "Wideband balanced-to-unbalanced filtering power dividers based on coupled lines," *IEEE Trans. Microwave Theory Tech.*, Vol. 65, No. 1, 86–95, Jan. 2017.
17. Zhu, H., J.-Y. Lin, and Y. J. Guo, "Filtering balanced-to-single-ended power dividers with wide range and high level of common-mode suppression," *IEEE Trans. Microwave Theory Tech.*, Vol. 67, No. 12, 5038–5048, Dec. 2019.
18. Feng, W., X. Ma, R. Gómez-García, Y. Shi, W. Che, and Q. Xue, "Multi-functional balanced-to-unbalanced filtering power dividers with extended upper stopband," *IEEE Trans. Circuits Syst. II Exp. Briefs*, Vol. 66, No. 7, 1154–1158, Jul. 2019.
19. Feng, W., W. Che, Y. Shi, Q. Xue, Y. C. Li, and X. Y. Zhou, "High selectivity balanced-to-unbalanced filtering power dividers using dual-mode ring resonators," *IEEE Trans. Compon., Packag., Manuf. Technol.*, Vol. 9, No. 5, 927–935, May 2019.
20. Wang, Z., Z. Zhu, Y. Fu, P. Han, H. Liu, and S. Fang, "A miniaturized balanced-to-unbalanced in-phase filtering power divider with wide upper stopband and wideband common-mode suppression," *IEEE Access*, Vol. 9, 143181–143187, Oct. 2021.
21. Lee, J., J. Lee, and N. S. Barker, "Rigorous design of input-reflectionless filter with Chebyshev response and exact approach to increase reflectionless range," *IEEE Trans. Microwave Theory Tech.*, Vol. 69, No. 10, 4460–4475, Oct. 2021.
22. Zhao, K., R. Gómez-García, and D. Psychogiou, "Tunable quasi-reflectionless bandpass filters using substrate integrated coaxial resonators," *IEEE Trans. Circuits Syst. II Exp. Briefs*, Vol. 69, No. 2, 379–383, Feb. 2022.
23. Zhang, Y., Y. Wu, W. Wang, and J. Yan, "High-performance common- and differential-mode reflectionless balanced band-pass filter using coupled ring resonator," *IEEE Trans. Circuits Syst. II Exp. Briefs*, Vol. 69, No. 3, 974–978, Mar. 2022.

24. Fan, M., K. Song, L. Yang, and R. Gómez-García, "Frequency-reconfigurable input-reflectionless bandpass filter and filtering power divider with constant absolute bandwidth," *IEEE Trans. Circuits Syst. II Exp. Briefs*, Vol. 68, No. 7, 2424–2428, Jul. 2021.
25. Lee, B., S. Nam, and J. Lee, "Filtering power divider with reflectionless response and wide isolation at output ports," *IEEE Trans. Microwave Theory Tech.*, Vol. 67, No. 7, 2684–2692, Jul. 2019.
26. Pan, B., W. Feng, Y. Shi, M. Huang, W. Che, and Q. Xue, "High-performance wideband balanced bandpass filter based on transversal signal-interference techniques," *IEEE Trans. Plasma Sci.*, Vol. 48, No. 12, 4119–4126, Dec. 2020.
27. Kwa1, H. W., X. M. Qing, and Z. N. Chen, "Broadband single-fed single-patch circularly polarized antenna for UHF RFID applications," *IEEE AP-S Int. Symp.*, 1–4, 2008.
28. Nghiem, X. A., J. Guan, and R. Negra, "Design of a broadband three-way sequential Doherty power amplifier for modern wireless communications," *IEEE MTT-S Int. Microwave Symp.*, 1–4, 2014.
29. Kang, H., H. Oh, W. Lee, C. S. Park, K. C. Hwang, K. Y. Lee, and Y. Yang, "Symmetric three-way Doherty power amplifier for high efficiency and linearity," *IEEE Trans. Circuits Syst. II Exp. Briefs*, Vol. 64, No. 8, 862–866, Aug. 2017.